Performance of polyaniline/manganese oxide-MWCNT Nanocomposites as Supercapacitors

Mir Ghasem Hosseini[a],*, Elham Shahryari[b]

[a,b] *(Department of Chemistry, University of Tabriz, Tabriz +98 4113393138, Iran*

Abstract

Composite electrodes of polyaniline/MnO_2-Multi walled carbon nanotube (PANI/MnO_2-MWCNT), MnO_2-MWCNT nanocomposites and MWCNT were produced by the *in situ* direct coating approach. The structure and morphology of the nanocomposites were studied by Fourier transform infrared (FT-IR) spectroscopy and scanning electron microscopy (SEM). The electrochemical properties of electrodes were also investigated by cyclic voltammetry (CV), galvanostatic charge–discharge and electrochemical impedance spectroscopy (EIS) techniques in 0.5 M Na_2SO_4. The specific capacitance of 321.47 F. g^{-1}, 277.77 F. g^{-1}, and 80 F. g^{-1} were obtained for PANI/MnO_2-MWCNT, MnO_2-MWCNT, and MWCNT, respectively. The EIS results also showed that the capacitive behavior of MWCNT was improved by the addition of MnO_2 and PANI.

Keywords: Chemical polymerization; supercapacitor; PANI/MnO_2-MWCNT; impedance; MnO_2

Introduction

Tremendous efforts have been devoted to the development of energy storage devices with high-energy density. Conventional dielectric capacitors have the limitation of low power [1]. Supercapacitors have attracted much attention due to their higher power density and long cycle life [1,2]. The energy storage of supercapacitors results from the charging or discharging of electrical double layer (electrical double layer capacitance) or from faradic redox reactions (pseudocapacitance)

*Corresponding author: M. G. Hosseini
Tel: +98 (41) 13393138, Fax: +98 (41) 13340191
E-mail: mg-hosseini@tabrizu.ac.ir

[3]. The capacitance of electrical double layer arises from the charge separation at the electrode-electrolyte interface of large surface area material such as activated carbon [4] or other nano structured carbon materials [5,6]. In contrast, pseudo-capacitor utilizes faradic redox process of different nanoparticles such as transition metal oxides [7,8] and conducting polymers [8]. To achive high performance supercapacitor based electrodes, combination of these three group materials can be used [9-12]. MnO_2 is considered to be one of the most promising transition metal oxides for the successive generation of supercapacitors due to its high-energy density, low cost, environmentally friendliness, and natural abundance [13-15]. However, literature survey reveals that the electrochemical properties of MnO_2 samples are limited by their low electrical conductivity. The specific capacitance of thin MnO_2 films is around 700 F. g^{-1}. However, the specific capacitance gradually reduces as the film thickness increases, and the reported values are usually in the range of 100 to 250 F. g^{-1} [16]. Thus, many approaches have been taken to overcome these disadvantages through synthesizing specific nanostructures [17-19] or composites with conducting materials. To utilize MnO_2 effectively, a popular strategy based on MnO_2/electrical

conductive materials has been exploited to improve the electrochemical performance. The binary or ternary composites of MnO_2/carbonaceous materials, MnO_2/conducting polymers or inorganics and MnO_2/carbon nanotubes/conducting polymers have recently been investigated [20]. To that end, researchers have made great efforts in developing conducting polymers as good candidates for supercapacitor electrode materials due to their unique properties such as facile thin film fabrication, ease of processability, light weight, and elasticity [21]. Among conducting polymers, polyaniline (PANI) has attracted significant attention because of its high electroactivity, controllable electrical conductivity, and excellent environmental stability [22].

In this work, we present a route to prepare hybrid electrodes in the form of PANI/MnO_2/MWCNT and MnO_2-MWCNT nanocomposites in two steps. The synergistic effect of MnO_2 and PANI on the supercapacitive behavior of MWCNT was studied. MnO_2 was deposited on MWCNT by the direct coating method and reducing $KMnO_4$, then PANI was deposited on it by oxidation polymerization. The electrochemical performance of PANI/MnO_2-MWCNT, MnO_2-MWCNT, and

MWCNT electrodes were investigated by electrochemical impedance spectroscopy, cyclic voltammetry, and galvanostatic charge– discharge techniques.

Experimental

Materials

Ammonium persulfate (APS) was obtained from Merk. Aniline monomer was distilled prior to its use. All other chemicals were of analytical grade and used as received. All electrochemical experiments were carried out at room temperature.

Procedures

Preparation of MnO_2-MWCNT

According to [23], first, 0.5 g of MWCNT was mixed with 100 mL of 0.2M $KMnO_4$ solution in a flask. The solution mixture was then refluxed at 140 °C while strring for 12h. After the reaction, the mixture was filtered and washed with distilled water to remove the residual $KMnO_4$. The filterate cake was redispersed in 200 mL of deionized water followed by the addition of 10 ml of 1M citric acid, and, then, maintained at 160 °C for 12 h under vigorous agitation during the whole course. A condenser was fitted to the reactor to prevent liquid loss from evaporating. Finally, the composite products were obtained through filtering, purifying with water, and drying processes.

Preparation of PANI/MnO_2-MWCNT

According to [23], first of all, 0.1 g of MnO_2-MWCNT was dispersed in 100 mL of 1M HCl solution under sonication for 1 h. Then, 5 ml of the aniline monomer was added to the MnO_2-MWCNT solution with constant stirring. After that, 100 mL of 0.1M APS solution was added dropwise to the above solution for 30 min to initiate oxidation polymerization. The reaction was continued for 24 h at 0 to 5 °C. Then, the final product was washed with water and acetone. Finally, the remaining powder was dried in oven at 80 °C for 24 h.

Preparation of the electrodes

In order to prepare the working electrodes, samples, carbon black, and polytetrafluroethylene (PTFE) were mixed (70:20:10, w/w) and dispersed in N-Methyl-2-pyrrolidone (NMP). The mixture was coated on graphite electrode (diameter=2mm, length=1.6cm and A=1.0048cm^2), and dried at 100 °C for 12 h.

## Characterization and electrochemical tests

Morphology of the nanocomposites was characterized with a scanning electron microscope (MIRA3FEG-SEM, Tescan). FT-IR spectra were recorded on Perkin-Elmer FT-IR spectrophotometer (4000–450 cm^{-1}). KBr pellet technique was used to prepare samples for recording FT-IR spectrum.

The electrochemical experiments were performed in a three electrode cell arrangement. A platinum sheet with a geometric area of about 20 cm^2 was used as a counter electrode, and the potentials were measured with respect to an Ag/AgCl reference electrode. Electrochemical experiments were carried out using a Princeton Applied Research, EG&G PARSTAT 2263 Advanced Electrochemical system run by PowerSuite software. Cyclic voltammetry measurements were carried out in 0.5 M Na$_2$SO$_4$ solution at a scan rate of 10 to 50 mV.s^{-1} in a voltage range of −1.0 to 1.0 V. Galvanostatic charge/discharge curves were measured at a current density of 0.2 A. g^{-1}. Electrochemical impedance measurements were carried out by applying an AC voltage of 10 mV amplitude in the 100 kHz to 10 mHz frequency range. Fit and analysis of EIS data were performed with ZSimTM 3.22 software.

Results and discussion

Material characterization

Studies of FTIR
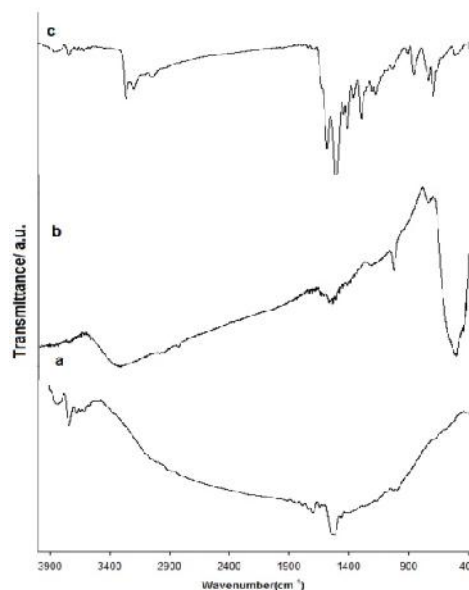
Figure 1. FTIR spectrum of a) MWCNT, b) MnO$_2$-MWCNT and c) PANI/MnO$_2$-MWCNT

Figure 1. shows the FT-IR spectra of MWCNT, MnO$_2$-MWCNT and PANI/MnO$_2$-MWCNT nanocomposites. Fig. 2(a) reveales a peak at around 1700cm^{-1} which is associated with the presence of C=O stretching mode of carboxylic groups. The peak observed at 3800 cm^{-1} is related to the OH group of carboxylic acid. From Fig. 1(b) the broadband at around 3400cm^{-1} and the one between 400 and 800cm^{-1} are attributed to the stretching vibrations of H–O–H and Mn–O bending vibration, respectively. Several small absorption peaks at around 1000–1500cm^{-1} are attributed to the bending vibrations of O–H bonds. The PANI/MnO$_2$-MWCNT nanocomposite (Figure 1(c)) shows the peaks of 1581cm^{-1}(assigned as C=C stretching of the quinoid rings), 1413 cm^{-1}

(C=C stretching deformation of benenzoid ring), 1294 cm^{-1} (C–N stretching of secondary aromatic amine), 1145 cm^{-1} (N–N quinoid), and 825 cm^{-1} (out-of-plane deformation C–H in the benzene ring) [24].

Morphological characterization

Figure 2 shows the SEM images of the MWCNT and MnO$_2$-MWCNT. MWCNT (Figure 2(a)) are in an aggregated form and have a smooth surface where the diameters are approximately 30 to 50 nm. Compared to MWCNT, MnO$_2$-MWCNT exhibits a rougher surface and is appeared as bright particles on the MWCNT [23]. MnO$_2$ causes MWCNT to be thicker than before.
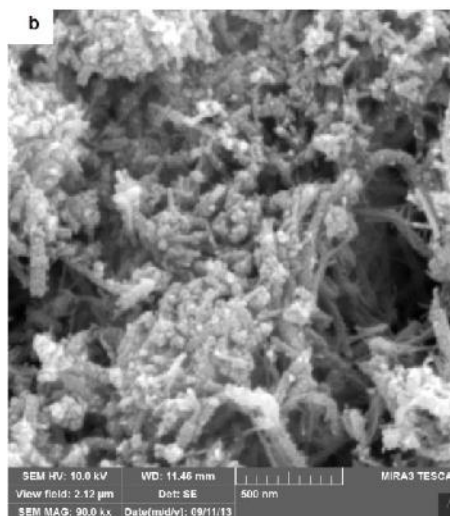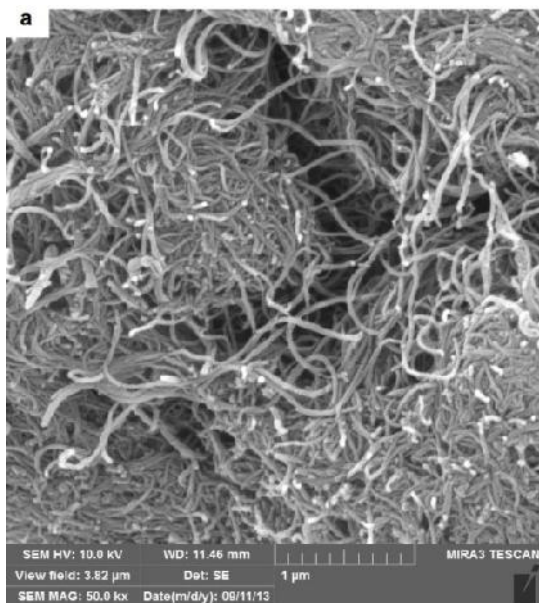
Figure 2. SEM images of a) MWCNT, b) MnO$_2$-MWCNT

To improve the electrical and electrochemical properties of MnO$_2$, MWCNT was used as the substrate for the nano-scaled MnO$_2$ layer. Besides, it can also provide a synergistic effect not found alone in neither MnO$_2$ nor MWCNT.

Electrochemical tests

Cyclic Voltammetry studies

Figure 3 depicts the typical voltammograms of the electrodes with the scan rate of 10 mV.s^1. The curves show rectangular mirror images with respect to the zero-current line, indicating the capacitive behavior. It can be clearly seen that the current density of MWCNT was increased by the incorporation of MnO$_2$ nanoparticles. Furthermore, the current density of MnO$_2$-MWCNT is also increased by application of PANI. It can be clearly seen that there are no redox peaks in

the working potential, also, the voltammograms of MWCNT and MnO_2-MWCNT are featureless and have symmetric characteristics of a supercapacitor [25].

The average specific capacitance values are calculated from the CV curves according to Eq. (1) [26].

$$C_{sp} = \frac{1}{m \cdot \upsilon \cdot \Delta V} \quad I_v \cdot dv \qquad (1)$$
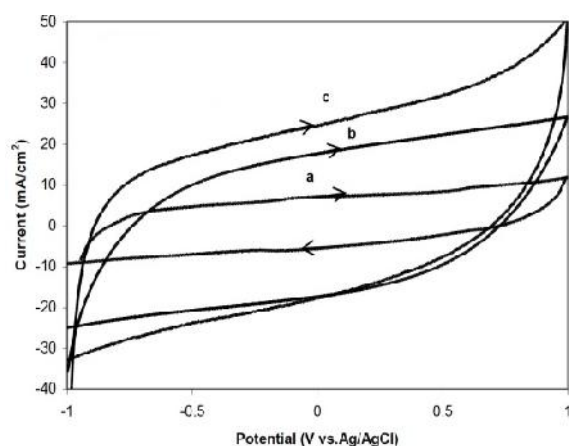
Figure 3. Cyclic voltametry of a) MWCNT, b) MnO_2-MWCNT, and c) PANI/MnO_2-MWCNT at 10 mV.s^{-1} in 0.5 M Na_2SO_4 solution

In the Eq.1, m is the mass of active material, *v* shows the potential scan rate, V shows the sweep potential window and I $_{(V)}$ is the voltammetric current on CV curves.
The capacitances deduced from the CV curves for the PANI/MnO_2-MWCNT, MnO_2-MWCNT and MWCNT electrodes were 321.47, 277.77 and 80 (F. g^{-1}), respectively.

Galvanostatic charge-discharge characteristics

Figure 4 shows the charge–discharge curves of PANI/MnO_2-MWCNT, MnO_2-MWCNT and MWCNT nanocomposites measured at a constant current of 0.2 A.g^{-1} within the potential window of -1.0 to 0.6 V vs. Ag/AgCl reference electrode.
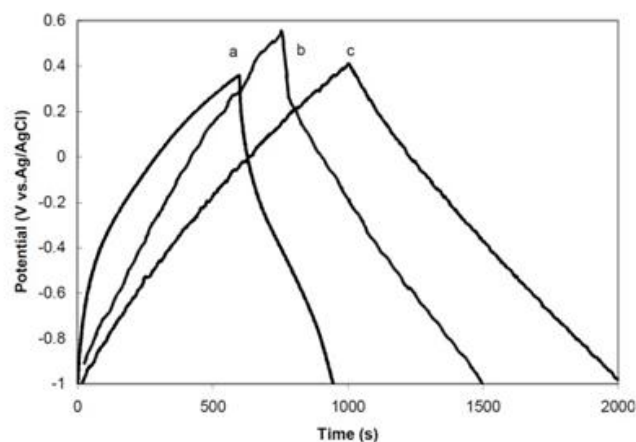
Figure 4. Charge–discharge behaviors of a) MWCNT, b) MnO_2- MWCNT, and c) PANI/MnO_2-MWCNT at 0.2 A/g in 0.5 M Na_2SO_4 solution

As shown in Figure 4(a), MWCNT is not in a triangular shape. It is clear that there is a small ohmic drop at the beginning of the discharge, and this clarifies that MWCNT has an Equivalent Series Resistance (ESR) [27]. For MnO_2-MWCNTnanocomposite in Figure 4(b) the curve shows ohmic drop at the beginning of the discharge process. This suggests that a part of current is consumed by ESR of the capacitor [28]. PANI/MnO_2-

MWCNT nanocomposite exhibits lower ohmic drop compared to the MnO_2-MWCNT and MWCNT. This indicates higher coulombic efficiency and reversible behavior. The charge/discharge duration of the first electrode is increased with the incorporation of MnO_2 and PANI. The specific capacitance of these nanocomposites based electrodes can be calculated according to the following equation (2):

$$C_{sp} = \frac{i}{(dV/dt.m)} \qquad (2)$$

Where, m is the mass of active material, i is the applied current, dV/dt is the rate of discharge after the IR drop [25,28]. The specific capacitance of PANI/MnO_2-MWCNT, MnO_2-MWCNT, and MWCNT was calculated to be 310, 230, 60 (F. g^{-1}), respectively.

The coulombic efficiency of the capacitor can be calculated from the galvanostatic charge–discharge experiments as follows [24,26]:

$$\eta = Q_d/Q_c \times 100 = \Delta t_d/\Delta t_c \times 100 \qquad (3)$$

In which, t_c and t_d are the duration of charge and discharge (s). According to Eq. (3) it can be derived that the average coulombic efficiency of PANI/MnO_2-MWCNT is around 98%.

Electrochemical Impedance Spectroscopy Analysis

EIS was also used to evaluate the supercapacitive performance and to study the electrochemical behavior of the electrodes. The electrochemical impedance of PANI/MnO_2-MWCNT, MnO_2-MWCNT, and MWCNT electrodes were examined over the frequency range of 100 kHz to 10 mHz in 0.5 M Na_2SO_4 .

The intersection of Nyquist plot at a high frequency with the real axis (Z) is the equivalent resistance of ionic resistance of the electrolyte, the intrinsic resistance of the substrate, and contact resistance between the active material and the current collector [25,29].

a)

b)
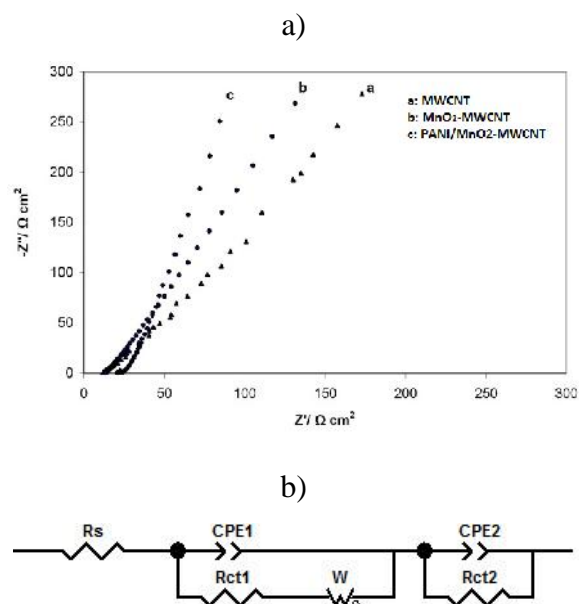
Figure 5. a) Impedance Nyquist plots of the electrodes b) equivalent circuit for the fitting of the EIS spectra of the electrodes

At low-frequency region, the plots almost have very sharp slopes, reflecting a pseudo-capacitor behavior with a high diffusion resistance. In the mid-frequency range, the electrodes behave as a parrallel configuration of a resistor and a capacitor. The imaginary part of the impedance which increases sharply by decreasing the frequency is an indicative of a faradaic process produced by the redox transitions of PANI and MnO_2 [30]. For the quantitative evaluation of different parameters of the electrodes, the experimental data were fitted to the equivalent circuit model (Figure 5(b)). This equivalent circuit is based on the following equations:

$$Z\omega = R_s + Z_1\omega \qquad (4)$$
$$+ Z_F(\omega)$$

$$\frac{1}{Z_1(\omega)} = \frac{1}{R_{ct1} + W} \qquad (5)$$
$$+ j\omega C_{dl}$$

$$\frac{1}{Z_F(\omega)} = \frac{1}{R_{ct2}} + j\omega C_F \qquad (6)$$

In these equations, , R_s, Z_1, Z_F, W, R_{ct}, C_{dl} and C_F are the angular frequency, solution resistance, impedance of electrode/electrolyte interface, bulk faradic impedance, Warburg diffusion impedance, ionic charge transfer resistance at the electrode/electrolyte interface, double layer capacitance, and bulk faradic pseudocapacitance. The CPE is obtained from [30]:

$$Z_{CPE} = \frac{1}{Y_0(j\omega)^\alpha} \qquad (7)$$

Where Y_0 and are the parameters that are independent of frequency. The exponent shows the roughness of the electrode , taking values from 0 to 1. In the case of = 1, CPE is equivalent to the capacitor while = 0 shows it behaves as a resistor, and for Warburg behavior = 0.5. The true capacitance from a depressed semicircle model (i.e. a constant phase element in parallel with a resistor) can be calculated by the following equation [31]:

$$C = \frac{(Q \times R)^{1}\,\alpha}{R} \qquad (8)$$

Where C, Q, R and indicate the specific capacitance (F. cm^{-2}), a constant with dimension (S. s), ionic charge-transfer resistance (. cm^2) is a constant without dimension, respectively. Table 1 shows the results of fitting the EIS data. It is obvious that the values of are close to 1, which in turn states the capacitive behavior of the electrodes.

One can infer from the Table 1 that C_2 is greater than C_1, which is in good agreement with the low thickness of the double layer. In the Table 1, it can be seen that for all the electrodes, R_{ct2} is greater than R_{ct1} that it results from the redox reactions of PANI or MnO_2 film, which in turn are much faster than the charge storage of MWCNT by

adsorption/desorption mechanism. With respect to their capacitance, the electrodes are ordered in a decrescent trend as follows:

$PANI/MnO_2$-MWCNT > MnO_2- MWCNT > MWCNT.

Table. 1. The best fitting values of the equivalent circuit elements in Figure 5(b) for the impedance data shown in Figure 5(a)

	Element									
	R_s (Ω)	Q_1 ($S.s^1$)	α_1	Rct_1 ($\Omega.cm^2$)	W ($\Omega.s^{-.5}$)	Q_2 ($S.s^2$)	α_2	Rct_2 ($k\Omega.cm^2$)	C_1 ($F.cm^{-2}$)	C_2 ($F.\,cm^{-2}$)
MWCNT	$13 \pm$ 0.00407	$0.11 \pm$ 0.01762	$0.8 \pm$ 0.00796	$103 \pm$ 0.01222	$0.002 \pm$ 0.16050	$0.85 \pm$ 0.07822	$0.8 \pm$ 0.00600	$5.81 \pm$ 0.02463	0.218	7.126
MnO_2-MWCNT	$12.1 \pm$ 0.02269	$0.10 \pm$ 0.04391	$0.7 \pm$ 0.01349	$108 \pm$ 0.02444	$0.2 \pm$ 0.01161	$0.8 \pm$ 0.061530	$0.82 \pm$ 0.01043	5.6 ± 0.04210	0.2773	5.065
PANI/MnO_2- MWCNT	$13 \pm$ 0.02638	$0.25 \pm$ 0.04177	$0.63 \pm$ 0.02049	$110 \pm$ 0.1010	$0.003 \pm$ 0.02287	$0.8 \pm$ 0.39640	$0.92 \pm$ 0.009095	6 ± 0.02588	1.751	1.772

Conclusion

PANI/MnO_2-MWCNT and MnO_2-MWCNT electrodes are prepared through *in situ* direct coating method to deposit MnO_2 and, subsequanetly, PANI on MWCNT. The structural and electrochemical properties of the nanocomposites were studied by FTIR, SEM, cyclic voltammetry, galvanostatic charge-discharge, and EIS techniques. Also, it was shown that the presence of PANI and MnO_2 would modify the supercapacitive behavior of MWCNT. The electrodes of PANI/MnO_2-MWCNT > MnO_2-MWCNT > MWCNT were ordered with respect to their specific capacitance, decreasingly. It was concluded that the specific capacitance raise is due to the synergistic effect of PANI and MnO_2.

References

[1] S. Kumar Mehr, P. Justin, G. RangaRao, *Appl. Mat. And Interfaces*, **2011**, *3,* 2063-2073.

[2] C.H. Yang, Y.S. Jang, H.K. Jeong, *Curr. Appl. Phys.*, **2014**, *14*, 1616-1620.

[3] B.E. Conway, *J Electrochem. Soc.,* **1991**, *138*, 1539-1542.

[4] B. Lee, J.R. Yoon, *Curr. Appl. Phys.*, **2013**, *13*, 1350-1353.

[5] F.J. Liu, T.F. Hsu, H. Yang, *J. Power Sources,* **2009**, *191*, 678-683.

[6] H.R. Ghennaatian, M.F. Mousavi, S.H. Kazemi, M. Shamsipur, *Syth. Met.,* **2009**, *159*, 1717-1722.

[7] Y.J. Lee, S. Park, J.G. Seo, J. R. Yoon, J. Yi, I.K. Song, *Curr. Appl. Phys.,* **2011**, *11*, 631-635.

[8] J. Liu, J. Essner, J. Li, *Chem. Mater.,* **2010**, *22*, 5022-5030.

[9] L. Mei, T. Yang, C. Xu, M, Zhang, L. Chen, Q. Li, T. Wang, *Nano Energy,* **2014**, *3*, 36-45.

[10] X. Zhang, L. Ji, S. Zhang, W. Yang, *J. Power Sources*, **2007**, *173*,1017-1023.

[11] E.N. Konyushenko and N.E. Kazantseva, J. Stejskal *et al.*, *J Magnetism Magnetic Mater,* **2008**, *320*, 231-240.

[12] A. Rudge, I. Raistrick, S. gottesfeld and J.P. Ferraris, *Electrochim. Acta,* **1994**, *39*, 273-287.

[13] K.W. Nam, C.W. Lee, X.Q. Yang, B.W. Cho, W.S. Yoon, K.B. Kim, *J. Power Sources,* **2009**, *188*, 323-331.

[14] H. Ashassi-Sorkhabi, E. Asghari, P. Laʾ le Badakhshan, *Curr. Appl. Phys.,* **2014**, *14*, 187-191.

[15] J.M. Ko, K.M. Kim, *Mater. Chem. Phys.,* **2009**, *114*, 837-841.

[16] P. Sen, A. De, *Electrochim. Acta,* **2010**, *55*, 4677-4684.

[17] A.E. Fischer, M.P. Saunders, K.A. Pettigrew, D.R. Rolison, J.W. Long, *J Electrochem. Soc.,* 2008, *155*, A246-A252.

[18] J. Wei, I. Zhitomirsky, *Sur. Eng.,* **2008**, *24*, 40-46.

[19] M. Cheong, I. Zhitomirsky, *Sur. Eng.,* **2009**, *25*, 346-352.

[20] J. Wang, Y. Yang, Z.H. Huang, F. Kang, *Electrochim. Acta,* **2012**, *75*, 213-219.

[21] S.I. Cho, S.B. Lee, *Dekker Encyclopedia of Nanoscience and Nanotechnology,* **2005**, *1*, 1-7.

[22] Z.A. Hu, Y.L. Xie, Y.X. Wang, H.Y. Wu, Y.Y. Yang, Z.Y. Zhang, L.P. Mo, *Mater. Chem. and Phys.,* **2009**, *114*, 990-995.

[23] K.S. Kim, S.J. Park, *J. of Solid State Electrochem.,* **2012**, *16*, 2751-2758.

[24] A. Mirmohseni, M.S. Seyed Dorraji, M.G. Hosseini, *Electrochim. Acta.,* **2012**, *70*, 182-192.

[25] Y.T. Wang, A.H. Lu, H.L. Zhang, **,** W.C. Li, *The J. of Phys. Chem. C,* **2011**, *115*, 5413-5421.

[26] P. Lv, P. Zhang, F. Li, Y. Feng, W. Feng, *Synthetic Met.,* **2012**, *162*, 1090-1096.

[27] A.M.P. Hussain, A. Kumar, *J. Power Sources,* **2006**, *161*, 1486-1492.

[28] J. Zhang, D. Shu, T. Zhang, H. Chen, H. Zhao, Y. Wang, Z. Sun, S. Tang, *J. of Alloys and Compd.,* **2012**, *532*, 1-9.

[29] Y. Li, K. Huang, D. Zeng, S. Liu, Z. Yao, *J. of Solid State Electrochem,* **2010**, *14*, 1205-1211.

[30] F. Gobal, M. Faraji, *Electrochim. Acta,* **2013**, *100*, 133-139.

[31] C.S. Hsu, F.Mansfeld, *Corrosion,* **2001***, 57*, 747-755.